INTERNATIONAL JOURNAL FOR NUMERICAL METHODS IN FLUIDS, VOL. 21, 981–991 (1995)

SPACE–TIME FINITE ELEMENT COMPUTATION OF COMPRESSIBLE FLOWS BETWEEN MOVING COMPONENTS

G. P. WREN

Weapons Technology Directorate, U.S. Army Research Laboratory, Aberdeen Proving Ground, MD 21005-5066, U.S.A.

AND

S. E. RAY, S. K. ALIABADI AND T. E. TEZDUYAR

Department of Aerospace Engineering and Mechanics and Army High Performance Computing Research Center, University of Minnesota, 1100 Washington Avenue South, Minneapolis, MN 55415, U.S.A.

SUMMARY

A numerical simulation capability for the injector flow of a regenerative liquid propellant gun (RLPG) is presented. The problem involves fairly complex geometries and two pistons in relative motion; therefore a stabilized space–time finite element formulation developed earlier and capable of handling flows with moving mechanical components is used. In addition to the specifics of the numerical method, its application to a 30 mm RLPG test firing is discussed. The computational data from the simulation of this test case are interpreted to provide information on flow characteristics, with emphasis on the tendency of the flow to separate from the injection orifice boundary of the test problem. In addition, the computations provided insight into the behaviour of the flow entering the combustion chamber.

KEY WORDS: finite elements; compressible flow; space–time formulation; moving components

1. INTRODUCTION

Recent advances in finite element strategies to solve compressible flow problems have allowed the equations describing challenging applied problems to be solved. The problems investigated in this paper involve nearly incompressible, barotropic flows. In particular, we are interested in orifice flows between moving mechanical components which are driven by large pressure differentials. Data describing such flows are limited and are often gathered far from the region of primary interest; thus, such data serve only to establish confidence in the model. Furthermore, the physics and dynamics of nearly incompressible flows at high pressure over complicated geometries are not yet fully understood. In particular, better understanding of thermal characteristics and the potential of the flow to remain attached to the boundary and to develop vortices is needed to design injectors for such flows.

Such problems pose a numerical challenge because the method must be able to handle complex, moving geometries and be sufficiently robust to handle the extreme range of flow conditions. The finite element method is ideally suited for this class of problems because of its inherent geometric flexibility. Since grid indexing is not necessary, unstructured grids which are often needed to effectively solve for flow fields over complex geometries are permitted. In addition, most calculations can be efficiently performed in an element-by-element fashion to carry out the large-scale, time-dependent, non-linear computations on supercomputers.

In the specific problem examined in this paper, the changes in the geometry of the problem require a formulation that can handle moving boundaries and interfaces. The deformable spatial

CCC 0271–2091/95/100981–11

Received 23 June 1994
Revised 14 August 1994

domain/stabilized space–time (DSD/SST) formulation introduced earlier[1,2] has this capability. This is an accurate, general-purpose, stabilized finite element formulation for computation of unsteady flow problems involving free surfaces, two-liquid interfaces, moving mechanical components and fluid–structure and fluid–particle interactions. In the DSD/SST method the stabilized finite element formulation of the governing equations is written over the space–time domain of the problem and therefore the deformation of the spatial domain with respect to time is taken into account automatically. Furthermore, with the advanced stabilization techniques used in the DSD/SST formulation, the numerical stability challenges involved in the problem are overcome without introducing excessive numerical dissipation and therefore with minimal loss of accuracy.

The applied problem of interest involves injector flow in the orifice of a regenerative liquid propellant gun (RLPG) studied by the Weapons Technology Directorate (WTD) of the U.S. Army Research Laboratory (ARL), Aberdeen Proving Ground, MD. In the RLPG a liquid monopropellant is injected at high pressure through the annulus formed by two moving pistons into the combustion chamber of the gun. Subsequently the propellant undergoes an intricate series of processes including jet break-up and combustion at gun pressures in the range 0·1–500 MPa over approximately 25 ms. Fluid flow from the liquid reservoir and through the injector may influence the jet behaviour as well as contribute to occasional flow reversal observed in experimental data.

Current U.S. Army injector designs have evolved empirically based on smooth, experimentally measured piston motion and mass flow rate requirements. In general, current designs have provided satisfactory results. However, modifications to the injector designs have been observed to yield unexpected effects in some tests, indicating a lack of fundamental understanding of fluid flow in the injector and conditions leading to flow separation and cavitation.

The mathematical modelling of this problem is based on the Navier–Stokes equations of compressible flows for the fluid, the equations governing the dynamics of moving components and the interface conditions governing the interaction between the fluid and the moving components. This results in a time-dependent, non-linear, partial differential equation system which needs to be solved over an intricate computational domain that changes its shape with time. The change in the shape of the computational domain is one of the unknowns of the problem and needs to be determined as part of the overall solution.

2. GOVERNING EQUATIONS

The compressibility of liquids is measured in terms of the bulk modulus, which gives the variation in pressure for a fractional change in density at a constant temperature:

$$K = \rho\left(\frac{\partial p}{\partial \rho}\right)_{\theta}. \tag{1}$$

Here K, p, ρ and θ are the bulk modulus, pressure, density and temperature respectively. For liquids the bulk modulus is typically very large (in the range of billions of pascals in our case), meaning that the compressibility is very small.

In problems where the pressure is of the same order of magnitude as the bulk modulus, such as in the RLPG, the compressibility of the working fluid plays an important role. Although the variations in density are small, they still lead to large variations in pressure. In such cases the liquid is usually modelled as a barotropic fluid. In barotropic fluids the pressure is assumed to be only a function of density. A simple equation of state which relates the pressure to the density can be obtained by assuming that the bulk modulus is a linear function of pressure:

$$K = K_1 + K_2 p, \tag{2}$$

where K_1 is the bulk modulus at zero gauge pressure and K_1 is a dimensionless constant. The solution of the differential equation (1) combined with (2) yields

$$p = \frac{K_1}{K_2}\left[\left(\frac{\rho}{\rho_0}\right)^{K_2} - 1\right]. \tag{3}$$

The barotropic fluid assumption decouples the energy equation from the governing equations, and the equations of conservation of mass and momentum suffice to describe the flow field characteristic of the RLPG. These equations in conservation law form can be written as

$$\frac{\partial \rho}{\partial t} + \nabla\cdot(\rho\mathbf{u}) = 0 \quad \text{on } \Omega_t \quad \forall t \in (0, T), \tag{4}$$

$$\frac{\partial(\rho\mathbf{u})}{\partial t} + \nabla\cdot(\rho\mathbf{u}\mathbf{u}) + \nabla p - \nabla\cdot T = \mathbf{0} \quad \text{on } \Omega_t \quad \forall t \in (0, T), \tag{5}$$

where T is the time period and Ω_t is the spatial domain at time t, with boundary Γ_t. Here $\mathbf{u}$ is the velocity and $\mathbf{T}$ is the Newtonian viscous stress tensor:

$$\mathbf{T} = \mu[\nabla\mathbf{u} + (\nabla\mathbf{u})^{\mathrm{T}}] + \lambda(\nabla\cdot\mathbf{u})\mathbf{I}, \tag{6}$$

$$\lambda = -\tfrac{2}{3}\mu. \tag{7}$$

In terms of conservation variables the axisymmetric version of equations (4) and (5) can be written as

$$\frac{\partial \mathbf{U}}{\partial t} + \frac{\partial \mathbf{F}_z}{\partial z} + \frac{\partial \mathbf{F}_r}{\partial r} + \frac{u_r}{r}\mathbf{U} - \nabla\cdot\mathbf{E} = \mathbf{0} \quad \text{on } \Omega_t \quad \forall t \in (0, T), \tag{8}$$

where $\mathbf{U} = (\rho, \rho u_z, \rho u_r)$ is the vector of conservation variables and $\mathbf{F}_z$, $\mathbf{F}_r$ and $\mathbf{E}$ are given as

$$\mathbf{F}_z = \begin{pmatrix} u_z\rho \\ u_z\rho u_z + p \\ u_z\rho u_r \end{pmatrix}, \qquad \mathbf{F}_r = \begin{pmatrix} u_r\rho \\ u_r\rho u_z \\ u_r\rho u_r + p \end{pmatrix}, \qquad \mathbf{E} = \begin{pmatrix} \mathbf{0} \\ \mathbf{T} \end{pmatrix}. \tag{9}$$

To provide a convenient set-up for our finite element formulation, equation (8) is written in the form

$$\frac{\partial \mathbf{U}}{\partial t} + \mathbf{A}_z\frac{\partial \mathbf{U}}{\partial z} + \mathbf{A}_r\frac{\partial \mathbf{U}}{\partial r} + \frac{u_r}{r}\mathbf{U} - \nabla\cdot\mathbf{E} = \mathbf{0} \quad \text{on } \Omega_t \quad \forall t \in (0, T), \tag{10}$$

where $\mathbf{A}_z$ and $\mathbf{A}_r$ are the Jacobians of $\mathbf{F}_z$ and $\mathbf{F}_r$ with respect to $\mathbf{U}$. Equation (10) is complemented with initial and boundary conditions of the form

$$\mathbf{U}(\mathbf{x}, 0) = \mathbf{U}_0 \quad \text{on } \Omega_0, \tag{11}$$

$$\mathbf{U}\cdot\mathbf{e}_k = g_k \quad \text{on } (\Gamma_t)_{g_k}, \quad k = 1, \ldots, n_{\mathrm{dof}}, \tag{12}$$

$$(\mathbf{E}\mathbf{n})\cdot\mathbf{e}_k = h_k \quad \text{on } (\Gamma_t)_{h_k}, \quad k = 1, \ldots, n_{\mathrm{dof}}, \tag{13}$$

where $\mathbf{e}_k$ is an orthonormal basis function in $\mathbb{R}^{n_{\mathrm{dof}}}$ and n_{dof} is the number of degrees of freedom, which in the current problem is three.

3. SPACE–TIME FINITE ELEMENT FORMULATION

The formulation used in this research is an axisymmetric extension of the formulation introduced in Reference 2. In the DSD/SST formulation we partition the time interval $(0, T)$ into subintervals

$I_n = (t_n, t_{n+1})$, where t_n and t_{n+1} belong to an ordered series of time levels $0 = t_0 < t_1 < \cdots < t_N = T$. Let $\Omega_n = \Omega_{t_n}$ and $\Gamma_n = \Gamma_{t_n}$. We define the space–time slab Q_n as the domain enclosed by the surfaces Ω_n, Ω_{n+1}, and P_n, where P_n is the surface described by the boundary Γ_t as t traverses I_n.

The finite element discretization of a space–time slab Q_n is achieved by dividing it into elements Q_n^e, $e = 1, 2, \ldots, n_{\text{el}}$, where n_{el} is the number of elements in the space–time slab Q_n. Based on this discretization, we define appropriate finite element function spaces $\mathscr{S}_n^h$ and $\mathscr{V}_n^h$ corresponding to the trial solutions and weighting functions respectively.

The DSD/SST formulation of equation (10) can be written as follows: start with

$$(\mathbf{U}^h)_0^- = \mathbf{U}_0^h, \tag{14}$$

and sequentially for $Q_1, Q_2, \ldots, Q_{N-1}$, given $(\mathbf{U}^h)_n^-$, find $\mathbf{U}^h \in \mathscr{S}_n^h$ such that $\forall \mathbf{W}^h \in \mathscr{V}_n^h$

$$\begin{aligned}
&\int_{Q_n} \mathbf{W}^h \cdot \left(\frac{\partial \mathbf{U}^h}{\partial t} + \mathbf{A}_z^h \frac{\partial \mathbf{U}^h}{\partial z} + \mathbf{A}_r^h \frac{\partial \mathbf{U}^h}{\partial r} + \frac{u_r^h}{r} \mathbf{U}^h \right) \mathrm{d}Q + \int_{Q_n} \nabla \mathbf{W}^h : \mathbf{E}^h \, \mathrm{d}Q + \int_{\Omega_n} (\mathbf{W}^h)_n^+ \cdot [(\mathbf{U}^h)_n^+ - (\mathbf{U}^h)_n^-] \, \mathrm{d}\Omega \\
&\quad + \sum_{e=1}^{(n_{\text{el}})_n} \int_{Q_n^e} \boldsymbol{\tau} \left(\frac{\partial \mathbf{W}^h}{\partial t} + (\mathbf{A}_z^h)^{\mathrm{T}} \frac{\partial \mathbf{W}^h}{\partial z} + (\mathbf{A}_r^h)^{\mathrm{T}} \frac{\partial \mathbf{W}^h}{\partial r} \right) \cdot \left(\frac{\partial \mathbf{U}^h}{\partial t} + \mathbf{A}_z^h \frac{\partial \mathbf{U}^h}{\partial z} + \mathbf{A}_r^h \frac{\partial \mathbf{U}^h}{\partial r} + \frac{u_r^h}{r} \mathbf{U}^h \right) \mathrm{d}Q \\
&\quad + \sum_{e=1}^{(n_{\text{el}})_n} \int_{Q_n^e} \delta \left(\frac{\partial \mathbf{W}^h}{\partial z} \cdot \frac{\partial \mathbf{U}^h}{\partial z} + \frac{\partial \mathbf{W}^h}{\partial r} \cdot \frac{\partial \mathbf{U}^h}{\partial r} \right) \mathrm{d}Q = \int_{(P_n)_{\text{h}}} \mathbf{W}^h \cdot \mathbf{h}^h \, \mathrm{d}P.
\end{aligned} \tag{15}$$

In the variational formulation given by (15), the following notation is used:

$$(\mathbf{U}^h)_n^{\pm} = \lim_{\epsilon \to 0} \mathbf{U}^h(t_n \pm \epsilon), \tag{16}$$

$$\int_{Q_n} (\ldots) \mathrm{d}Q = \int_{I_n} \int_{\Omega_t} (\ldots) \, \mathrm{d}\Omega \, \mathrm{d}t, \tag{17}$$

$$\int_{P_n} (\ldots) \mathrm{d}P = \int_{I_n} \int_{\Gamma_t} (\ldots) \, \mathrm{d}\Gamma \, \mathrm{d}t. \tag{18}$$

In this formulation the first three integrals together with the right-hand-side integral represent the time-discontinuous Galerkin formulation of the problem. The third integral enforces weakly, the continuity of the conservation variables across the space-time slabs. The first series of element-level integrals in equation (15) represents the SUPG stabilization terms and the second series represents the shock-capturing terms added to the formulation. The definition of the stabilization coefficients used in this formulation can be found in Reference 3.

4. DESCRIPTION OF THE RLPG

The RLPG is a propulsion concept under exploration by the U.S. Army which utilizes a liquid monopropellant as the fuel instead of traditional solid propellants. A schematic diagram of the interior of the gun is shown in Figure 1. The liquid propellant is loaded into the liquid reservoir behind the pistons before the firing cycle commences. To initiate the regenerative process, gas from an external source (not shown in the figure) raises the combustion chamber pressure. The inside piston, referred to as the control piston, moves first in response to the rise in combustion chamber pressure and its motion is modulated by a mechanically controlled damper in the rear of the gun. The outside piston, referred to as the injection piston, follows the motion of the control piston due to the differential area on the liquid reservoir and combustion chamber sides of the piston. Thus the motion of the two pistons is independent, although coupled via the liquid and combustion chamber pressures.

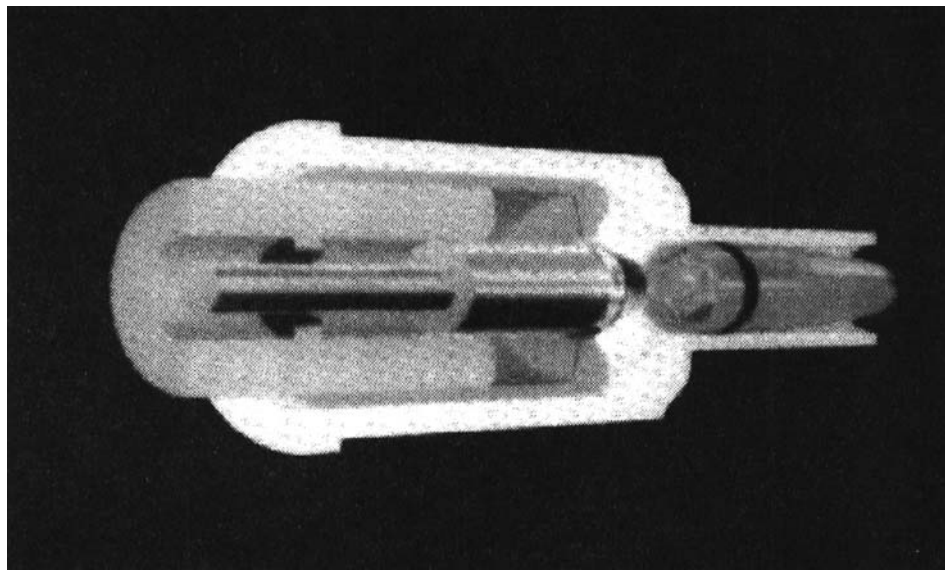

Figure 1. Regenerative liquid propellant gun (RLPG)

The liquid propellant in the reservoir flows through the annulus created between the two pistons into the combustion chamber where it combusts, raising the combustion chamber pressure and accelerating the projectile. An attractive feature of this design is that the flow of the propellant is inherently modulated by conditions in the liquid resorvoir and combustion chamber. For example, if the combustion chamber pressure rises rapidly, the injection piston will move faster, reducing the supply of propellant to the combustion chamber, lowering the combustion chamber pressure and re-establishing the pressure balance between the liquid reservoir and the combustion chamber. This is possible as long as a positive pressure gradient is maintained between the liquid reservoir and the combustion chamber.

Many injector geometries have been researched to promote smooth fluid flow and to minimize the risk of pressure gradient reversals. In the problem discussed in this paper, we investigate the geometry associated with a 30 mm RLPG, i.e. the bore of the gun has a diameter of 30 mm, fired at the WTD/ARL. The geometry of the reservoir and the orifice of the RLPG are axisymmetric.

During the routine firing cycle of the RLPG, only the liquid propellant is present in the injector region. Vaporization of the propellant and combustion of this vapour occur some distance downstream of the injector in the combustion chamber. It is therefore reasonable to assume that the local effects from such phase changes in the region of interest will be small enough to model the flow through the injector as a single-phase flow. Furthermore, since heat transfer and temperature changes in the liquid propellant in the reservoir are also expected to be small,[4] the energy equation can be left out of the analysis.

In the experimental firing the propellant used is XM46, a monopropellant composed of hydroxyl ammonium nitrate, triethanol ammonium nitrate and water. The physical properties of the propellant have been extensively investigated and the propellant compressibility at gun conditions cannot be ignored. Thus a compressible equation of state (3) for XM46 is implemented with coefficients $K_1 = 5350$ MPa, $K_2 = 9{\cdot}11$ and $\rho_0 = 1430$ kg/m^3 (see reference 5).

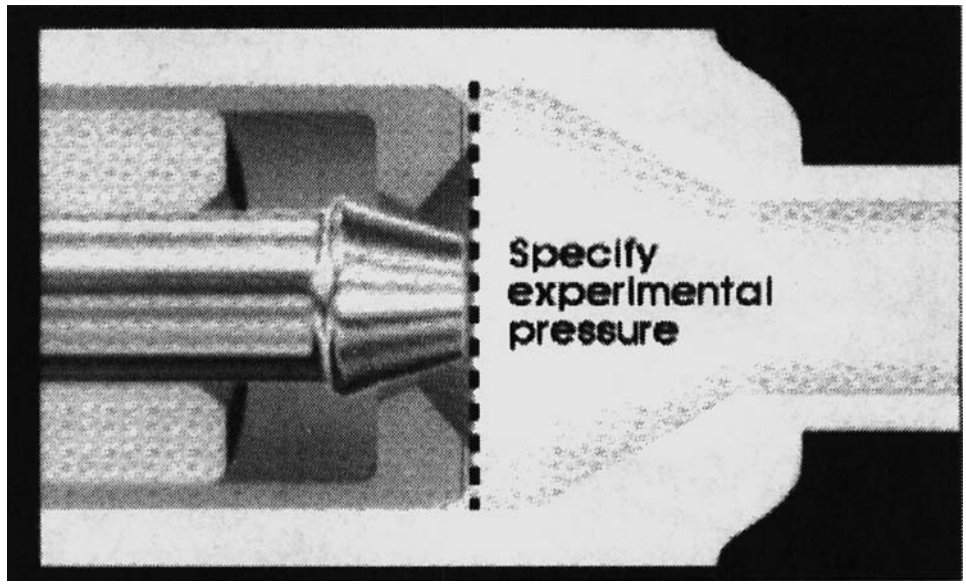

Figure 2. RLPG liquid reservoir, injector, combustion chamber and beginning of tube

5. NUMERICAL SIMULATION OF THE INJECTOR REGION OF THE 30 mm RLPG

5.1. Piston motion and boundary conditions

The liquid reservoir, injection orifice, combustion chamber and a portion of the bore are shown in Figure 2. As indicated in the diagram, the computational domain does not include the entire combustion chamber. The right-hand boundary of the domain in the combustion chamber is placed a short distance, compared with the length of the combustion chamber, from the nose of the inner piston. There are two principles guiding the placement of this boundary.

Despite the absence of combustion in the model, the effect of physical combustion occurring in the combustion chamber must be included. This is accomplished through the choice of the boundary conditions on the right-hand boundary. The mean, experimental chamber pressure is imposed here as measured by the pressure gauge mounted in the chamber wall nearest to this region. Placing this boundary in the interior of the chamber means that the pressure is imposed near where the data were recorded. In addition, the location represents a position at which fluid expansion and interaction with the gas are expected to induced atomization and subsequent combustion.

Secondly, this boundary is placed downstream far enough so that recirculation zones occurring on the chamber side of the pistons can be captured. However, these recirculation zones, combined with the pressure variation on this boundary, are enough to cause inflow through a stationary boundary. To minimize the effects of inflow, this boundary moves with the inner piston towards the rear of the gun as the simulation of the firing cycle proceeds.

The pistons and walls of the gun are assumed to be rigid, undergoing no deformation during the simulation. In the physical system the motion of the inner (control) piston is governed by the fluid pressure on its surface and a damper located behind the transducer block in the rear of the gun. To prevent the otherwise necessary simulation of the damper, the motion of the control piston is also taken from experimental data. The motion of the outer (injection) piston is computed based on the mass of the piston and the pressure forces acting on it. Viscous forces, since they are small compared with the pressure forces, are neglected in computing the motion of the injection piston. On all solid walls in the domain, no-slip boundary conditions are imposed.

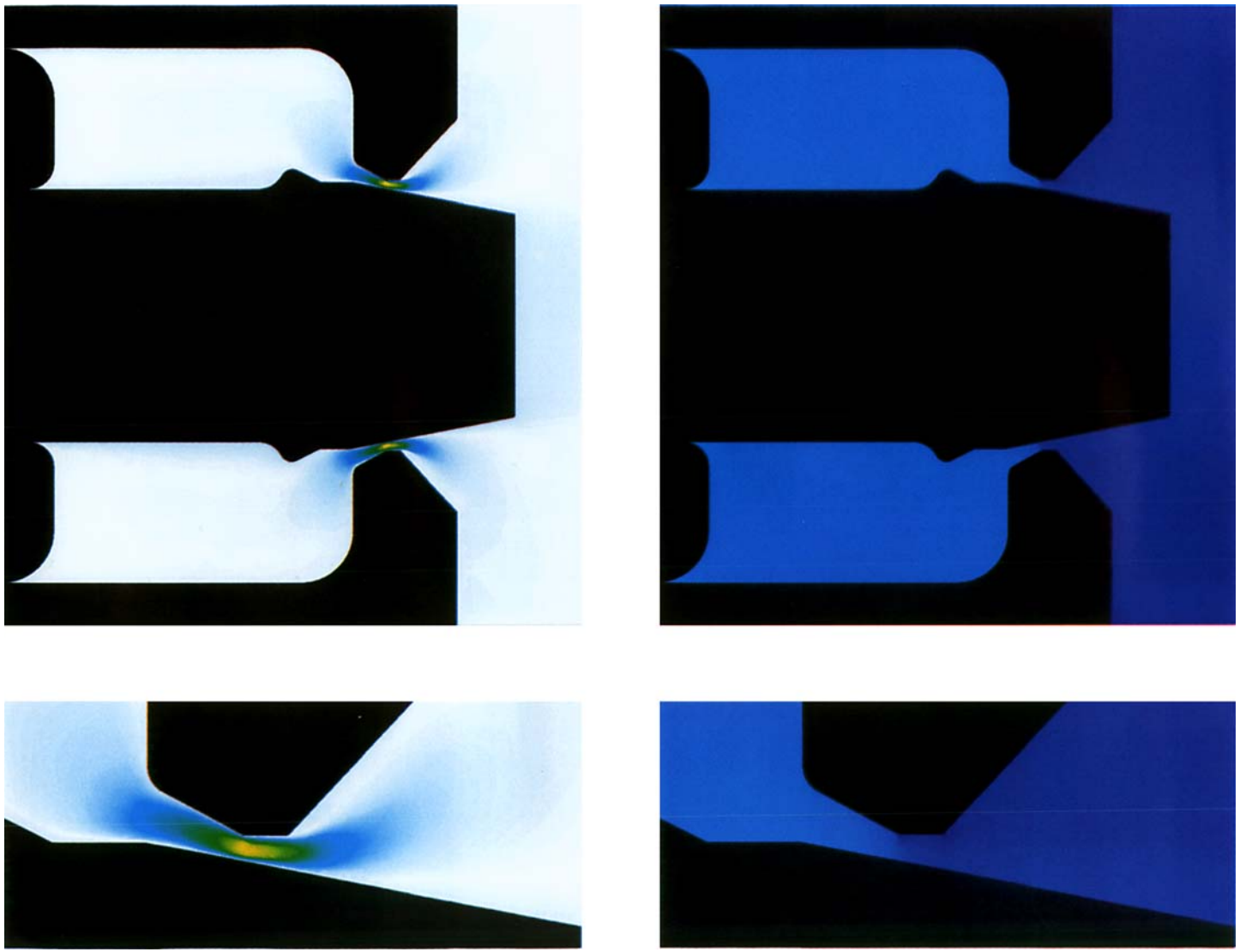

Plate 1. Mach number (left) and pressure (right) at $t = 7{\cdot}2$ ms

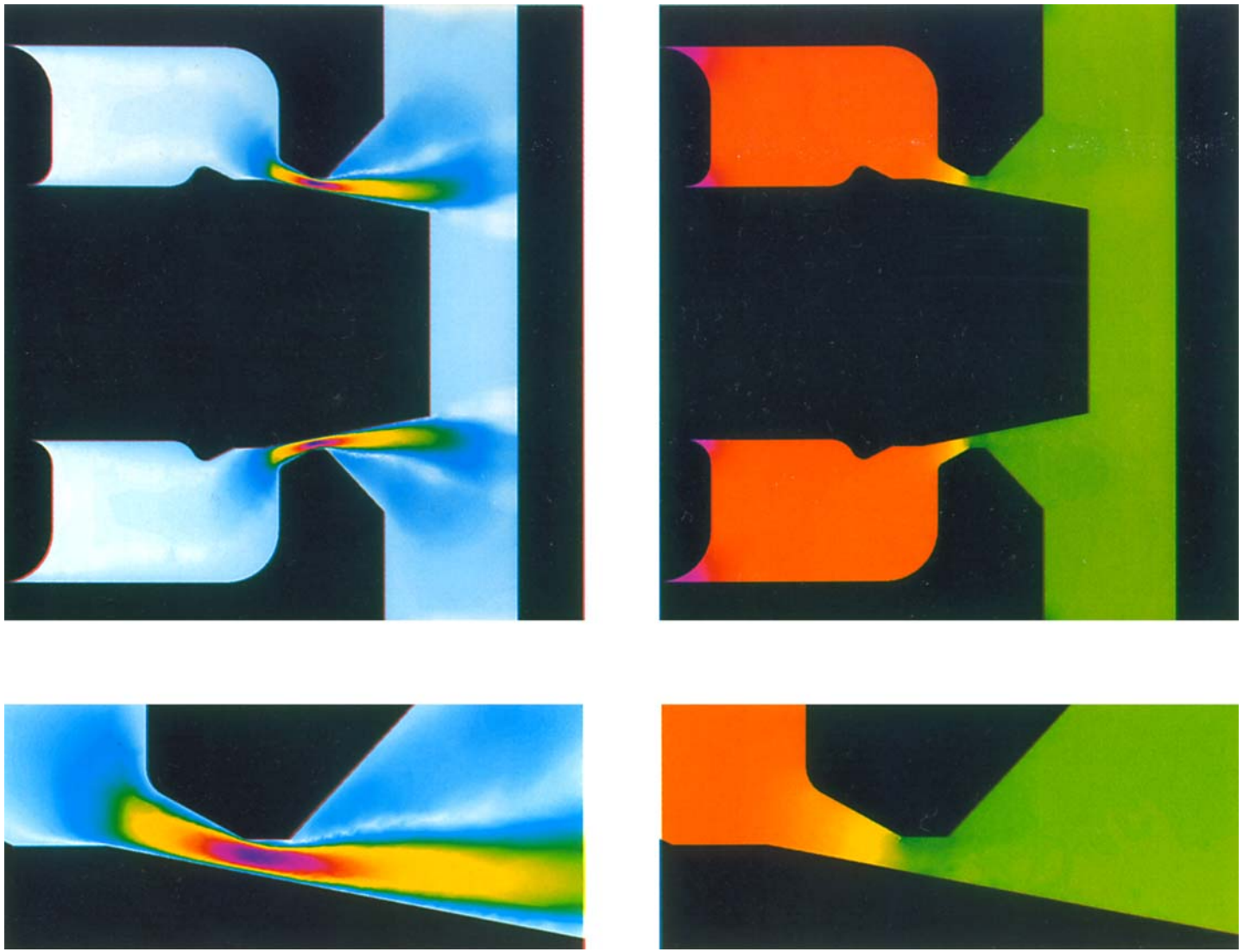

Plate 2. Mach number (left) and pressure (right) at $t = 8{\cdot}9$ ms

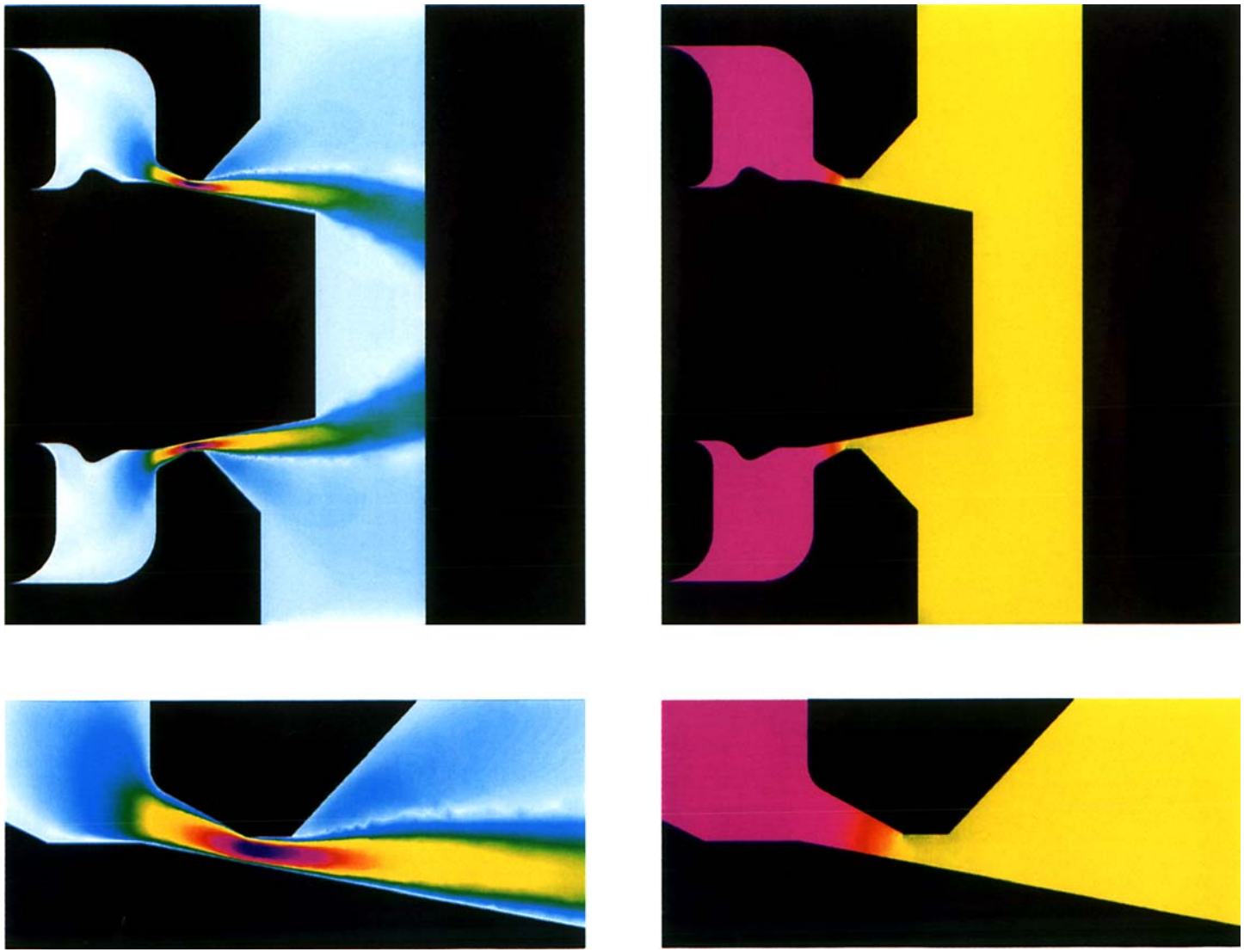

Plate 3. Mach number (left) and pressure (right) at $t = 10{\cdot}6$ ms

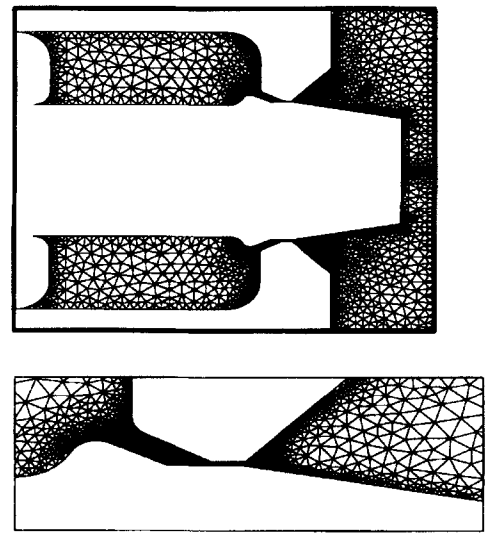

Figure 3. Mesh at $t = 4{\cdot}4$ ms

5.2. Mesh update strategy

The finite element mesh over the initial configuration of the computational domain is shown in Figure 3. This mesh was created with an automatic mesh generator to give a Delaunay-type mesh.[6] The changes in the geometry of the problem due to the motions of the pistons require the finite element mesh to be updated every time step. This is achieved by using a mesh update strategy that minimizes the frequency of remeshing. In the DSD/SST formulation the mesh is updated in such a way that remeshing is performed only when it becomes necessary to do so to prevent unacceptable degrees of mesh distortion. In this case, at each time step of the computations, an automatic mesh-moving scheme[7] is used to update the mesh as the pistons move. This automatic mesh-moving scheme is based on moving the mesh with the nodal displacements governed by the equations of elasticity. The motions of the pistons enter as boundary conditions associated with these equations. The computational domain still needs to be remeshed periodically to prevent excessive deformation of the mesh.

Figures 4–6 show the mesh at $t = 7{\cdot}2$, $8{\cdot}9$ and $10{\cdot}6$ ms respectively. During the time interval between $7{\cdot}2$ and $8{\cdot}9$ ms the pistons move with roughly the same velocity and therefore the mesh in the orifice area does not undergo a significant deformation. The mesh in the reservoir area, on the other hand, undergoes the largest deformation. Still, no remeshing takes place during this time interval and therefore the meshes shown in Figures 4 and 5 have the same number of elements and nodes (6126 elements and 3295 nodes) and the same connectivity. One remeshing takes place in the time interval between the images depicted in Figures 5 and 6, with the mesh in Figure 6 having 6626 elements and 3523 nodes. As the orifice closes in the later part of the firing cycle, the mesh generator creates smaller elements within this region in order to still be able to capture the dynamics in this region. This results in a refined grid in the neighbourhood of the orifice and the increase in the number of elements and nodes between Figures 5 and 6. The meshes used in this simulation range in sizes of 5800–8000 elements and 3150–4250 nodes. Again, this large range of mesh sizes is attributable to the variation in size of the orifice.

5.3. Non-linear time-dependent computations and initial conditions

Approximately 20,000 coupled non-linear fluid dynamics equations are solved at each time step. In addition, at each time step, linear equations governing the motions of the piston and mesh need to be

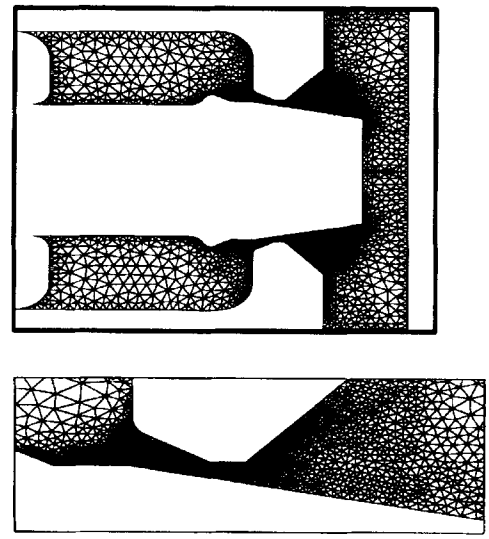

Figure 4. Mesh at $t = 7{\cdot}2$ ms

solved. Multiple iterations are required to solve these equations at each time step because of the non-linearity of the fluid dynamics equations and also the coupling between the fluid flow and the piston and mesh motions. Depending on the selection of the initial conditions for the simulation, several iterations (up to 10) are needed during the first few time steps of the firing cycle. After that, typically two iterations per time step are sufficient.

The selection of the initial conditions in this simulation needs particular attention. In the actual operation of the RLPG the pistons are initially touching, sealing the reservoir from the combustion chamber. Also initially the reservoir is prepressurized and the chamber is at atmospheric pressure. No attempt is made in this simulation to model the contact between the pistons and therefore the simulation is started with a finite gap between them. Keeping this gap small, with only one or two

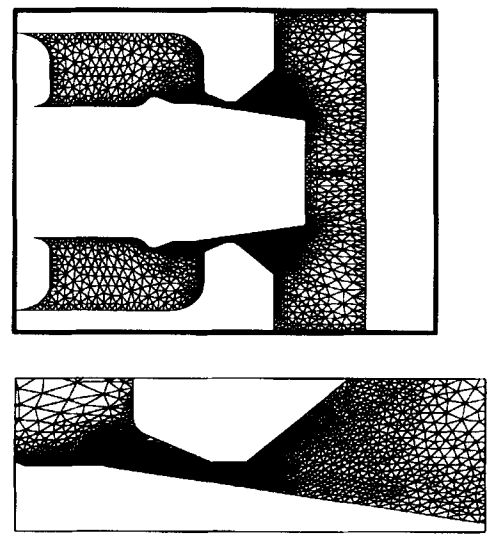

Figure 5. Mesh at $t = 8{\cdot}9$ ms

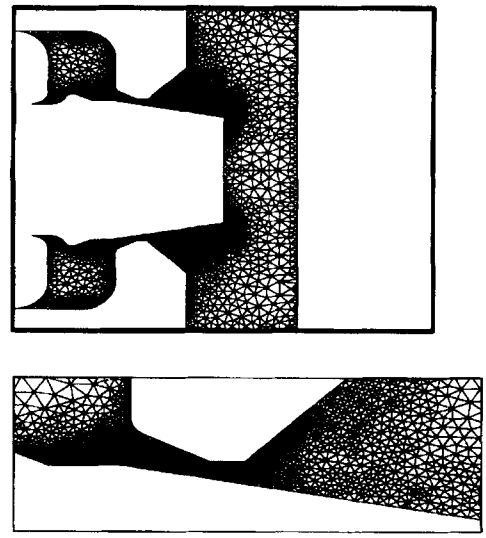

Figure 6. Mesh as $t = 10{\cdot}6$ ms

elements across, numerically chokes the flow in the orifice and approximates the desired effect of having no flow through the orifice at the beginning. The initial conditions for pressure are generated by setting the reservoir pressure to the prepressurization value of the propellant and the chamber pressure to atmospheric pressure. For the purpose of setting the initial conditions, the pressure between these two regions is assumed to vary linearly over the length of the orifice.

5.4. Results

The simulation begins at a time $t = 4{\cdot}4$ ms in the experimental data. In the test firings, during the time span from 0·0 to 4·4 ms, the ignition sequence takes place, which is not of interest to this study. However, in keeping with the timing of the experimental firing cycle, this initial time was chosen.

To compare the computations from the DSD/SST model with those from the test firings of the 30 mm RLPG, the results are compared with those from a lumped parameter model of the gun,[5] which agree quite well with the experimental liquid, combustion chamber and damper pressures. The lumped parameter model was chosen for the comparison because there is some uncertainty in the experimental measurement of the piston positions. The calculated pressure at the centre of the transducer block at a

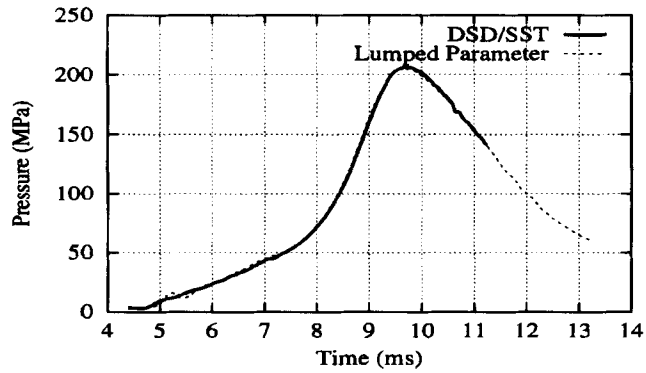

Figure 7. Pressure at transducer block: lumped parameter model of experiment and DSD/SST prediction

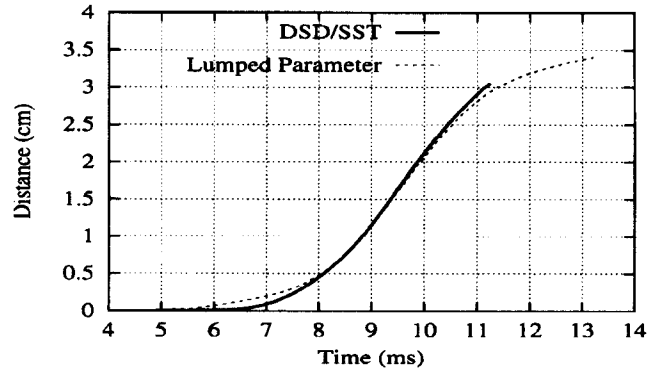

Figure 8. Motion of injector piston: lumped parameter model of experiment and DSD/SST prediction

location corresponding to the position of the experimental liquid pressure gauge is compared with that from the lumped parameter model in Figure 7 and the agreement is quite favourable. Also, the motion of the injection piston from the current solution is compared with that from the lumped parameter code in Figure 8. Although the agreement is not as good as the comparison in liquid pressure, it is considered adequate to establish confidence in the DSD/SST model.

Plates 1–3 show the Mach number and pressure at the three instants mentioned earlier, namely $t = 7{\cdot}2$, 8·9 and 10·6 ms respectively. Early in the firing cycle the flow outside of the injector follows the contour of the outer piston as the fluid enters the combustion chamber at low speed. As the injection cycle progresses and the flow becomes fully developed with a higher velocity, a recirculation zone appears on the chamber side of the outer piston. Interestingly, at both times the fluid appears to lift from the inner piston just downstream of the injection orifice. Thus the inner piston nose may be exposed to hot gases during the combustion process. However, we acknowledge that the computation does not include a model for jet break-up and combustion and that the observations discussed above may be modified in the actual gun environment.

We now focus on the detailed view of the Mach number in the orifice shown below the full view of the computational domain in Plates 1–3. The Mach number of the flow through the injection orifice formed by the smallest area between the two pistons is highest, as expected, and acceleration of the fluid can be seen at the injector entrance. A detailed examination of the Mach number distribution reveals that the flow shows no tendency to separate from either piston until after it passes through the orifice. This is desirable since flow separation upstream of the orifice may otherwise allow hot combustion gases to move into the orifice or even into the reservoir. This phenomenon is referred to as flow reversal and may lead to propellant ignition in these regions.

The pressure images show that there is a very small pressure gradient from the rear to the front of the liquid reservoir, as expected, and a large gradient in the orifice as seen in the detailed view. The lack of an adverse pressure gradient and the small radial gradient compared with the axial gradient are also indications that the specific geometry of the injection orifice is well-designed for the nominal chamber pressure history imposed in the simulation.

6. CONCLUDING REMARKS

We have demonstrated that the numerical methods developed earlier for computation of compressible flow problems with moving mechanical components can be effectively applied to the simulation of the regenerative liquid propellant gun (RLPG). The stabilized, space–time finite element formulation employed here is capable of handling the complex geometries, moving pistons and large pressure

variations involved in this problem. Although we have reported in this paper only results from the simulation of the 30 mm RLPG, the techniques have also been applied to other RLPG configurations.[8] Based on these simulations, the methodology appears to be a sufficiently reliable diagnostic and design tool for injectors in the RLPG.

ACKNOWLEDGEMENTS

This research was sponsored by NASA-JSC under grant NAG 9-449, by NSF under grant CTS-8796352 and by ARPA under NIST contract 60NANB2D1272. Partial support for this work has also come from ARO contract number DAAL03-89-C-0038 with the AHPCRC at the University of Minnesota. Cray C90 time was provided in part by the Minnesota Supercomputer Institute.

REFERENCES

1. T. E. Tezduyar, M. Behr and J. Liou, 'A new stratetgy for finite element computations involving moving boundaries and interfaces—the deforming-spatial-domain/space–time procedure: I. The concept and the preliminary tests', *Comput. Methods Appl. Mech. Eng.*, **94**, 339–351 (1992).
2. S. K. Aliabadi and T. E. Tezduyar, 'Space–time finite element computation of compressible flows involving moving boundaries and interfaces', *Comput. Methods. Appl. Mech. Eng.*, **107**, 209–224 (1993).
3. S. K. Aliabadi and T. E. Tezduyar, 'Parallel fluid dynamics computations in aerospace applications', *Int. j. numer. methods fluids*, **21**, 783–805 (1995). (This volume.).
4. T. P. Coffee, 'An updated lumped parameter code for regenerative liquid propellant in-line guns', *Tech. Rep. BRL-TR-2974*, Ballistic Research Laboratory, 1988.
5. T. P. Coffee, G. P. Wren and W. F. Morrison, 'A comparison between experiment and simulation for concept VIC regenerative liquid propellant guns. I. 30 mm', *Tech. Rep. BRL-TR-3072*, Ballistic Research Laboratory, 1989.
6. A. A. Johnson, 'Mesh generation and update strategies for parallel computation of flow problems with moving boundaries and interfaces', *Ph.D. Thesis*, Department of Aerospace Engineering and Mechanics, University of Minnesota, Minneapolis, MN, 1995.
7. T. Tezduyar, S. Aliabadi, M. Behr, A. Johnson and S. Mittal, 'Massively parallel finite element computation of three-dimensional flow problems', *Proc. 6th Jpn. Numerical Fluid Dynamics Symp.*, Tokyo, 1992, pp. 15–24.
8. S. E. Ray, 'Large-scale computational strategies for solving compressible flow problems,' PhD. Thesis, Department of Aerospace Engineering and Mechanics, University of Minnesota, Minneapolis, MN, 1995.